Interatomic Coulomb interaction and electron nematic bond order in FeSe

Kun Jiang, Jiangping Hu, Hong Ding, and Ziqiang Wang

Phys. Rev. B **93**, 115138 — Published 23 March 2016

DOI: 10.1103/PhysRevB.93.115138

Interatomic Coulomb interaction and electron nematic bond order in FeSe

Kun Jiang,[1] Jiangping Hu,[2] Hong Ding,[2] and Ziqiang Wang[1]

[1] *Department of Physics, Boston College, Chestnut Hill, MA 02467, USA*
[2] *Institute of Physics, Chinese Academy of Sciences, Beijing 100190, China*

(Dated: March 4, 2016)

Despite having the simplest atomic structure, bulk FeSe has an observed electronic structure with the largest deviation from the band theory predictions among all Fe-based superconductors and exhibits a low temperature nematic electronic state without intervening magnetic order. We show that the Fe-Fe interatomic Coulomb repulsion V offers a natural explanation for the puzzling electron correlation effects in FeSe superconductors. It produces a strongly renormalized low-energy band structure where the van Hove singularity sits remarkably close to Fermi level in the high-temperature electron liquid phase as observed experimentally. This proximity enables the quantum fluctuations in V to induce a rotational symmetry breaking electronic bond order in the d-wave channel. We argue that this emergent low-temperature d-wave bond nematic state, different from the commonly discussed ferro-orbital order and spin-nematicity, has been observed recently by several angle resolved photoemission experiments detecting the lifting of the band degeneracies at high symmetry points in the Brillouin zone. We present a symmetry analysis of the space group and identify the hidden antiunitary T-symmetry that protects the band degeneracy and the electronic order/interaction that can break the symmetry and lift the degeneracy. We show that the d-wave nematic bond order, together with the spin-orbit coupling, provide a unique explanation of the temperature dependence, momentum space anisotropy, and domain effects observed experimentally. We discuss the implications of our findings on the structural transition, the absence of magnetic order, and the intricate competition between nematicity and superconductivity in FeSe superconductors.

PACS numbers:

I. INTRODUCTION

The electron nematic phase with purely rotational symmetry breaking is arguably the most unconventional and poorly understood phase in Fe-based superconductors. In the Fe-pnictides, the direct observation of nematic electronic structure has been difficult since the orthorhombic lattice distortion is immediately followed by the collinear spin density wave (SDW) order that breaks, in addition to the spatial-orbital rotational symmetry, lattice translation, spin-rotation, and time-reversal symmetries. This leaves the origin of nematicity highly debated [1] between the spin-nematic [2, 3] and ferro-orbital order [4–8] scenarios. In contrast, the Fe-chalcogenide FeSe undergoes the tetragonal to orthorhombic structural transition at $T_s = 87K$ and the SC transition at $T_c = 9K$ without any trace of magnetic order [9, 10]. The latter enabled direct observations of a rotational symmetry breaking electronic structure at low temperatures by several angle resolved photoemission spectroscopy (ARPES) experiments recently [11–15], unveiling that the SC transition in bulk FeSe takes place from a highly unconventional nematic electronic state. Understanding the microscopic origin of this nematic order, its relation to the structural transition and magnetism is the focus of this work.

In a nutshell, ARPES detects the splitting of symmetry protected degeneracies between the d_{xz} and d_{yz} orbitals in the band dispersions at the high symmetry points $\mathrm{M}(\pi, 0, 0)$ and the $\Gamma(0, 0, 0)/\mathrm{Z}(0, 0, \pi)$ in the original Brillouin zone (BZ). More importantly, the corresponding degeneracy splitting energy Δ_M and $\Delta_{\Gamma/Z}$ appear *anisotropic* in momentum space with different temperature dependence. The nematic transition is determined by the strongly T-dependent Δ_M whose onset coincides with [12, 13] or is about 20K above the structural transition T_s [11, 14]. Δ_M rises with decreasing T and reaches $\Delta_M \simeq 62$meV at 22K, closely resembling the T-dependence of an energy scale associated with a symmetry breaking order parameter. This is consistent with NMR [16, 17], optics, and transport measurements [18, 19] detecting changes in the electronic state near or above T_s. The splitting at the BZ center, $\Delta_\Gamma \simeq 30$meV at 22K, on the other hand, does not break rotational symmetry above T_s. It is nearly T-independent up to 150K and insensitive to T_s and the onset of Δ_M [14]. It was thus conjectured [14] that the nematic order in FeSe is not due to the commonly discussed ferro-orbital order [16, 20, 21], but rather driven by a d-wave nematic bond order [22] $O_{\mathrm{dNB}} = \sum_k (\cos k_x - \cos k_y)[n_{xz}(k) + n_{yz}(k)]$.

We show in this work that the nearest neighbor Fe-Fe interatomic Coulomb repulsion V can be the microscopic origin for the emergent nematic order, the absence of magnetism, and at a more fundamental level, the unusually large band renormalization in bulk FeSe. The observed electronic structure of FeSe shows the largest deviation from the local density approximation (LDA) band dispersions among all Fe-based superconductors [23, 24]. A remarkable difference from the Fe-pnictides is that the renormalization is the strongest at low energies near the Fermi level (E_F) as shown in Fig. 1, where the LDA bands are compared with ARPES measurements. Of crucial importance is the symmetry protected van Hove singularity (vHS) at M point created by the saddle point in

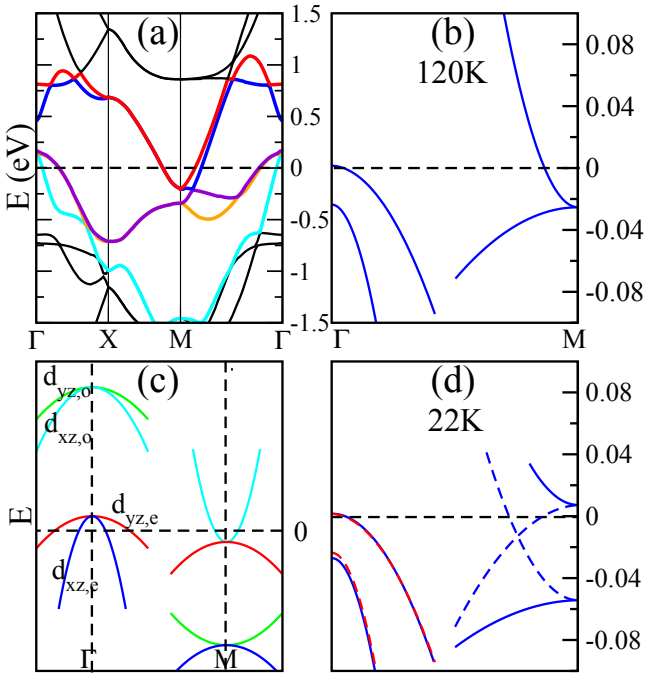

FIG. 1: (a) LDA band structure of FeSe.(b) Band dispersions observed by ARPES in the symmetric phase at 120K. (c) Band degeneracy at high symmetry points (Γ, M) among $d_{xz,e}$ (blue), $d_{yz,e}$ (red), $d_{xz,o}$ (cyan), and $d_{yz,o}$ (green). (d) ARPES results in the nematic state at 22K. Red dashed lines near Γ are data taken at 120K, showing Δ_Γ is nearly T-independent. Solid and dashed blue lines near M correspond to the two domains.

the band dispersions of the $d_{xz/yz}$ orbital. Being more than 250meV below E_F in LDA, it moves to a mere $E_{\rm vH} \simeq 25$meV below the Fermi level in ARPES in the high temperature electron liquid phase at $T > T_s$. We show that this correlation-induced proximity of the vHS to E_F, concomitant with the large mass enhancement and the contraction of the FS pockets, sets the stage for the electronic nematic transition near T_s that would ultimately gap out the vHS and induce the structural transition.

What is the microscopic interaction that would drive the vHS so close to E_F in the high-temperature electron liquid phase? The more than 10 times reduction in the distance from the hole band top at Γ to the vHS at M (see Fig.1) cannot come from crystal field corrections induced by local interactions [25, 26] since it comes from the same atomic orbital. Recent LDA+DMFT (dynamical meanfield theory) calculations [27, 28] show that the intra-atomic Hubbard U and Hund's rule coupling J would only produce a bandwidth reduction (albeit with some orbital dependence) and a mass enhancement by a factor of $3 \sim 4$ and leave the FS pockets much larger than those observed by ARPES and quantum oscillations [13]. Thus, intra-atomic correlations alone cannot account for the electronic structure near E_F [21].

We find that the nearest neighbor Coulomb V generates directly hopping corrections to the band dispersion: it pushes the vHS at M up toward E_F and pulls down the top of the hole band at Γ, resulting in a low energy dispersion consistent with experiments. Both the FS pockets and the $E_{\rm vH}$ in ARPES can be produced by a $V \simeq 0.73$eV in the Hartree-Fock (HF) theory with the bare LDA bandwidth $W \simeq 4.2$eV. When the vHS is driven to E_F (i.e. $E_{\rm vH} = 0$), a nematic instability of the Pomeranchuk-type occurs in the symmetry breaking valence bond channels. The leading instability corresponds precisely to the d-wave nematic bond order. The proximity to this nematic instability in bulk FeSe allows us to carry out a weak-coupling analysis of the extended t-U-V Hubbard model and find good agreement with experiments. Moreover, we find that the V-renormalized low-energy band structure with the reduced FS pockets promotes the d-wave nematicity while suppressing the collinear SDW, which is a possible explanation for the absence of magnetic order in bulk FeSe.

Since the symmetry content of the band degeneracies and its relation to the nematic order in Fe-based superconductors have not been understood, we begin in Section II with a systematic symmetry analysis. We show that the band degeneracy at the high symmetry point originates from the existence of two-dimensional irreducible representations of the space group involving rotation, reflection, and glide symmetries [29]. We then show that there exists two sets of "hidden" antiunitary T-symmetries (borrowing the T from an analogy to the time-reversal symmetry) that protect the band degeneracies at the Γ and M points respectively. All possible degeneracy lifting interactions are then studied according to their symmetry and symmetry-breaking properties in connection to the experimental findings on the temperature dependence, momentum space anisotropy, and domain effects. The analysis shows that the only interactions consistent with the experimental findings are the atomic spin-orbit coupling governing the lifting of the degeneracy at Γ without breaking the four-fold rotation symmetry, and the rotational symmetry breaking d-wave nematic bond order that splits the degeneracy at M. In Section III, we develop the microscopic theory for the nematic state in bulk FeSe based on the t-U-V Hubbard model and show that the quantum fluctuations in the intersite correlation V leads to the important band renormalization and in particular to the dynamical V-driven proximity of the vHS to the Fermi level. The nematic instability is studied in detail and the obtained low energy band structure and the Fermi surfaces are compared to recent experimental results. In Section IV, we provide a summary and discuss the implications of these findings on FeSe films, the effects of electron doping, and the interplay between nematicity and superconductivity, as well as propose experimental tests for the theory.

II. BAND DEGENERACY, SYMMETRY CONTENT, AND EFFECTIVE INTERACTIONS

We begin with a discussion on the symmetry-protected band degeneracies at the Γ and M points illustrated in Fig.1(c). These symmetry properties dictate a rich and interesting set of possible degeneracy lifting interactions with different implications on the momentum space anisotropy and the domain effects. We will show that only the d-wave nematic bond order is naturally consistent with the experimental findings for the nematic transition.

The LDA electronic structure (Fig.1a) can be described by the tight-binding (TB) model down-folded to the Fe 3d-manifold [30, 31],

$$H_t = \sum_{\sigma ij\alpha\beta} t_{ij}^{\alpha\beta} d^\dagger_{i\alpha\sigma} d_{j\beta\sigma} + \sum_{\sigma i\alpha} \varepsilon_\alpha d^\dagger_{i\alpha\sigma} d_{i\alpha\sigma}, \qquad (1)$$

where ε_α is the on-site (crystal field) energy of an electron in orbital $\alpha = (1,2,3,4,5) \equiv (xz, yz, x^2-y^2, xy, z^2)$ and $t_{ij}^{\alpha\beta}$ is the electron hopping integral between sites (i,j) and orbitals (α,β). The FeSe lattice structure contains two Fe atoms per unit cell labeled by $\ell = A$ and B. As a result, the TB Hamiltonian in momentum space is,

$$H_t = \sum_{k\sigma} \psi^\dagger_\sigma(k) H_t(k) \psi_\sigma(k), \qquad (2)$$

where the basis vector $\psi_\sigma(k) = [d^A_\sigma(k), d^B_\sigma(k)]^T$ with $d^\ell_\sigma = (d^\ell_{1\sigma}, d^\ell_{2\sigma}, \ldots, d^\ell_{5\sigma})$, and $H_t(k)$ is a 10×10 matrix whose eigenvalues govern the dispersion of the 10 LDA bands,

$$H_t(k)|n,k\rangle = E^n_k |n,k\rangle, \qquad n = 1\ldots 10. \qquad (3)$$

The explicit form of $H_t(k)$ and its parameters were derived in Refs.[23, 31] for FeSe. Note that to avoid confusion, we use the k values confined to the reduced two-Fe BZ shown in Fig.2(b) to label the momentum eigenstates such that the four M points are located at $(\pm\pi, 0)$ and $(0, \pm\pi)$ of the original one-Fe BZ.

A. Symmetry protected band degeneracies

The band degeneracies at Γ and M are related to three important space group symmetries $R \equiv S_4, \Sigma_d, G_s$ of the atomic and electronic structure in Fe-based superconductors. The most commonly discussed is the $S_4 = \Sigma_z \cdot C_4$ where a four-fold rotation C_4 is followed by a mirror reflection about the x-y plane to account for the staggering positions of the Se/As ions above and below the Fe-plane. The spatial-orbital operations of S_4 is therefore

$$\begin{aligned} S_4: \quad x &\to y, y \to -x, z \to -z, \\ d^\ell_{xz} &\to -d^\ell_{yz}, d^\ell_{yz} \to d^\ell_{xz}, d^\ell_{xy} \to -d^\ell_{xy}, \\ d^\ell_{x^2-y^2} &\to -d^\ell_{x^2-y^2}, d^\ell_{z^2} \to d^\ell_{z^2}. \end{aligned} \qquad (4)$$

The less discussed point group symmetry Σ_d is a mirror reflection about the diagonal xy-z plane and operates in the spatial and orbital space according to,

$$\begin{aligned} \Sigma_d: \quad x &\to y, y \to x, z \to z, \\ d^\ell_{xz} &\to d^\ell_{yz}, d^\ell_{yz} \to d^\ell_{xz}, d^\ell_{xy} \to d^\ell_{xy}, \\ d^\ell_{x^2-y^2} &\to -d^\ell_{x^2-y^2}, d^\ell_{z^2} \to d^\ell_{z^2}. \end{aligned} \qquad (5)$$

We will show that Σ_d plays as important a role as S_4 in the origin of the band degeneracy. Finally, the glide symmetry [32] of the space group $G_s = \Sigma_z \cdot T_{x,y}$ is associated with the translation by one lattice spacing along the x or y direction ($T_{x,y}$) followed by a mirror reflection about the x-y plane. Under the $G_s = \Sigma_z \cdot T_x$ operation, $A \leftrightarrow B$ and

$$\begin{aligned} G_s: \quad x &\to x+a, y \to y, z \to -z \\ d^A_{xz} &\to -d^B_{xz}, d^A_{yz} \to -d^B_{yz}, d^A_{xy} \to d^B_{xy}, \\ d^A_{x^2-y^2} &\to d^B_{x^2-y^2}, d^A_{z^2} \to d^B_{z^2}. \end{aligned} \qquad (6)$$

Since R is a symmetry of $H_t(k)$, $[H_t(k), R] = 0$. Thus, $R|n,k\rangle = |n',k'\rangle$ is a simultaneous eigenstate of $|n,k\rangle$ at the same energy E^n_k as given in Eq.(3). Note that in general $k' = Rk \neq k$. In particular, using Eqs. (4,5,6), it is simple to show that in momentum space:

$$\begin{aligned} S_4: k_x &\to -k_y, k_y \to k_x \\ \Sigma_d: k_x &\to k_y, k_y \to k_x \\ G_s: k_x &\to k_x, k_y \to k_y \end{aligned} \qquad (7)$$

However, at certain high symmetry points in the BZ (e.g. Γ and M), it is possible to have k' equal or equivalent to k under the reciprocal lattice vector, resulting in symmetry related band degeneracies. To elucidate this, we transform the basis vector in Eq. (2) into the eigenbasis of the glide symmetry operator G_s via a unitary rotation $\Psi_\sigma(k) = U\psi_\sigma(k) = U[d^A_\sigma(k), d^B_\sigma(k)]^T$ [32], where $U = \frac{1}{\sqrt{2}} \begin{pmatrix} U_1 & U_2 \\ U_1 & -U_2 \end{pmatrix}$ and

$$U_1 = \begin{pmatrix} 1&0&0&0&0 \\ 0&1&0&0&0 \\ 0&0&1&0&0 \\ 0&0&0&1&0 \\ 0&0&0&0&1 \end{pmatrix}, U_2 = \begin{pmatrix} 1&0&0&0&0 \\ 0&1&0&0&0 \\ 0&0&-1&0&0 \\ 0&0&0&-1&0 \\ 0&0&0&0&-1 \end{pmatrix}.$$

The rotation mixes the orbitals defined on the A and B sublattices and turns them into the corresponding even-odd combinations, $d^{e/o}_\alpha = \frac{1}{\sqrt{2}}(d^A_\alpha \pm d^B_\alpha)$, that form the eigenstates of G_s with ∓ 1 eigenvalues: $\Psi_\sigma(k) = [d^-_\sigma(k), d^+_\sigma(k)]^T$ where

$$d^{-/+}_\sigma = (d^{e/o}_{xz\sigma}, d^{e/o}_{yz\sigma}, d^{o/e}_{x^2-y^2\sigma}, d^{o/e}_{xy\sigma}, d^{o/e}_{z^2\sigma}). \qquad (8)$$

Since $[H_t(k), G_s] = 0$, U block-diagonalizes $H_t(k)$ in the $\Psi_\sigma(k)$ basis,

$$H_k = U H_t(k) U^\dagger = \begin{pmatrix} P(k) & 0 \\ 0 & P(k+Q) \end{pmatrix}, \qquad (9)$$

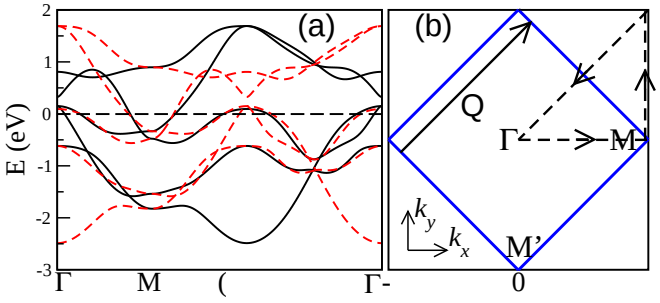

FIG. 2: (a) TB band of FeSe. Black solid lines are from $P(k)$ and red dashed lines are from $P(k+Q)$. (b) BZ of FeSe. The larger zone bounded by the black lines is the one-Fe BZ while the smaller zone with blue boundaries is the two-Fe BZ. Q corresponds to one of reciprocal lattice vectors in the two-Fe BZ. The dashed black lines with arrows indicate the trajectory over which the band dispersions are plotted in (a).

where $Q=(\pi,\pi)$ is the reciprocal lattice vector for the two-Fe unit cell. Eqs. (8) and (9) show that the lattice translation symmetry corresponds to their invariance under $k\to k+Q$, provided the exchange $e\leftrightarrow o$ is executed in orbital space [33]. This results in the important identification $|d^e_{\alpha\sigma},M'\rangle=|d^o_{\alpha\sigma},M'+Q\rangle=|d^o_{\alpha\sigma},M\rangle$ in the two-Fe zone. Diagonalizing $P(K)$ gives rise to five band dispersions with -1 eigenvalue under glide operation, and shifting them by $k\to k+Q$ generates the other five with $+1$ eigenvalue under G_s. These 10-bands are shown in Fig.2(a) for FeSe by the solid and the dashed lines respectively. Note that the band degeneracies at Γ are between the eigenstates within $P(k)$ (odd under G_s) or within $P(k+Q)$ (even under G_s), whereas the degeneracies at M are between the eigenstates of $P(k)$ and $P(k+Q)$.

On general grounds, the *two-fold* band degeneracies indicate that the space group of a Hamiltonian H must have at least one two-dimensional irreducible representation. Specifically, there must exist at least two group generators, representable by two matrices D_1 and D_2 with $[H,D_1]=[H,D_2]=0$, that are mutually noncommuting, $[D_1,D_2]\neq 0$. For the noninteracting system described by the TB Hamiltonian H_t, these two symmetries are manifestly the S_4 and Σ_d. When interactions are included, the degeneracies will remain so long as a pair of $D_{1,2}$ exist and the two-dimensional irreducible representation remains intact. For symmetry-breaking interactions that reduce the space group down to an abelian group with only one-dimensional representations, the band degeneracies will be lifted as we will show below.

Since the Hamiltonian H_k in Eq. (9) is manifestly diagonal and the states in Eq. (8) are the eigenstates at Γ and M points [29], the interplay between symmetry and band degeneracy can be studied by focusing on the $d^{e/o}_{xz}$ and $d^{e/o}_{yz}$ orbitals at Γ and M points separately. Eq. (8) shows that the degeneracies at Γ are within the e-e and o-o pairs, i.e. $|d^e_{xz}/d^e_{yz},\Gamma\rangle$ and $|d^o_{xz}/d^o_{yz},\Gamma\rangle$, whereas those at the M point, with the M' folded to M by the reciprocal lattice operation discussed above, are between the e-o components $|d^o_{xz}/d^e_{yz},M\rangle$ and $|d^e_{xz}/d^o_{yz},M\rangle$ as shown in Fig.1(c). These degeneracies clearly originate from the S_4 and the Σ_d symmetries defined in Eqs.(4) and (5) since,

$$\begin{aligned} S_4|d^e_{xz},\Gamma\rangle &= -|d^e_{yz},\Gamma\rangle, \quad S_4|d^e_{yz},\Gamma\rangle=|d^e_{xz},\Gamma\rangle,\\ \Sigma_d|d^e_{xz},\Gamma\rangle &= |d^e_{yz},\Gamma\rangle, \quad \Sigma_d|d^e_{yz},\Gamma\rangle=|d^e_{xz},\Gamma\rangle, \end{aligned}$$

and similarly for the odd components at Γ; and

$$\begin{aligned} S_4|d^e_{xz},M\rangle &= -|d^o_{yz},M\rangle, \quad S_4|d^e_{yz},M\rangle=|d^o_{xz},M\rangle.\\ \Sigma_d|d^e_{xz},M\rangle &= |d^o_{yz},M\rangle, \quad \Sigma_d|d^e_{yz},M\rangle=|d^o_{xz},M\rangle, \end{aligned}$$

and similarly when "e" and "o" are interchanged at M, which is equivalent to M' under the reciprocal lattice vector. More importantly, it is crucial that the two symmetries do not commute, i.e. $[S_4,\Sigma_d]\neq 0$ such that they form the two-dimensional irreducible representation of the space group necessary for the two-fold degeneracy.

For a deeper understanding that will facilitate the classification of the possible degeneracy-lifting interactions, let's recall the eigenbasis of the glide symmetry Ψ_σ and Eq. (8). In the decoupled subspace of xz and yz orbitals, $\Psi_\sigma=(d^e_{xz\sigma},d^o_{xz\sigma},d^e_{yz\sigma},d^o_{yz\sigma})^T$. It is convenient to regard this four-spinor as the direct product of two two-spinors spanning the orbital space (xz/yz) and the sublattice space (e/o). In the rest of the discussion, the spin indices are suppressed for notational simplicity unless otherwise noted. The TB Hamiltonian H_k in Eq. (9) can thus be written down explicitly up to constants at Γ and M points,

$$H_\Gamma=\lambda_\Gamma\sigma_0\otimes\tau_z, \quad H_M=\lambda_M\sigma_z\otimes\tau_z, \tag{10}$$

where σ_i and τ_i are Pauli matrices acting in the orbital and sublattice spaces, respectively; and λ_Γ and λ_M are half the energy separations between the pair of degenerate points at Γ and M. In this representation, the symmetry operators are

$$\begin{aligned} (S_4,\Sigma_d,G_s)_\Gamma &= (-i\sigma_y\otimes\tau_0,\sigma_x\otimes\tau_0,\sigma_0\otimes\tau_z), \quad (11)\\ (S_4,\Sigma_d,G_s)_M &= (-i\sigma_y\otimes\tau_x,\sigma_x\otimes\tau_x,\sigma_0\otimes\tau_z). \quad (12) \end{aligned}$$

They commute with $H_{\Gamma/M}$ correspondingly.

Next, we show that the band degeneracies at Γ and M are protected by nonunitary symmetries in very much the same way that the time-reversal symmetry protects the Z_2 topological insulators [34]. Note that the direct product of the Pauli matrices comprises the identity and 15 generators. A given $H_0=H_{\Gamma/M}$ anticommutes with 8 of the other 14 operators and commutes with the remaining 6. Remarkably, the 8 operators organize into two sets of 4 operators; each forms an independent Clifford algebra with H_0 and is protected by the hidden antiunitary symmetry T_1 or T_2 with $T^2_{1,2}=-\mathbf{1}$ respectively. We can therefore group the generators according to the following

$$\begin{array}{lccccc} & \underbrace{H_0,} & \underbrace{H_1,\ldots,H_4,} & \underbrace{H_5,\ldots,H_8,} & \underbrace{H_9,\ldots,H_{14},} & \\ T_1: & \text{even} & \text{even} & \text{odd} & \text{odd} & \\ T_2: & \text{even} & \text{odd} & \text{even} & \text{odd} & \end{array} \tag{13}$$

where $[H_0, H_{9,\ldots,14}] = 0$, and

$$\begin{aligned}
&\{H_0, H_{1,\ldots,4}\} = 0, \quad T_1 H_{0,1,\ldots,4} T_1^{-1} = H_{0,1,\ldots,4},\\
&\{H_0, H_{5,\ldots,8}\} = 0, \quad T_2 H_{0,5,\ldots,8} T_2^{-1} = H_{0,5,\ldots,8},\\
&T_1 H_{5,\ldots,14} T_1^{-1} = -H_{5,\ldots,14},\\
&T_2 H_{1,\ldots,4,9,\ldots 14} T_2^{-1} = -H_{1,\ldots,4,9,\ldots 14}.
\end{aligned} \tag{14}$$

Thus, the two-fold degeneracy of the quantum states at Γ and M in H_0 is protected by at least one necessary nonunitary symmetry $T \in (T_1, T_2)$, analogous to Kramers doublet $(|\alpha\rangle, T|\alpha\rangle)$ protected by the global nonunitary time-reversal symmetry. Specifically, we find that for H_Γ,

$$T_1^\Gamma = i\sigma_y K \otimes \tau_0, \quad T_2^\Gamma = i\sigma_y K \otimes \tau_z, \tag{15}$$

where K is the complex conjugation operator. They are effective time-reversal operators in the orbital angular momentum channel embedded symmetrically and antisymmetrically into the sublattice space respectively. Operators that are even under $T_{1,2}^\Gamma$ are

$$\begin{aligned}
T_1^\Gamma - \text{even}: &\quad H_\Gamma, \sigma_0 \otimes \tau_x, \sigma_x \otimes \tau_y, \sigma_y \otimes \tau_y, \sigma_z \otimes \tau_y\\
T_2^\Gamma - \text{even}: &\quad H_\Gamma, \sigma_0 \otimes \tau_y, \sigma_x \otimes \tau_x, \sigma_y \otimes \tau_x, \sigma_z \otimes \tau_x.
\end{aligned}$$

Similarly for H_M at M point,

$$T_1^M = \sigma_x \otimes i\tau_y K, \quad T_2^M = i\sigma_y K \otimes \tau_x, \tag{16}$$

and

$$\begin{aligned}
T_1^M - \text{even}: &\quad H_M, \sigma_x \otimes \tau_0, \sigma_y \otimes \tau_0, \sigma_z \otimes \tau_x, \sigma_z \otimes \tau_y,\\
T_2^M - \text{even}: &\quad H_M, \sigma_y \otimes \tau_z, \sigma_x \otimes \tau_z, \sigma_0 \otimes \tau_x, \sigma_0 \otimes \tau_y.
\end{aligned}$$

The identification of the antiunitary T-symmetries that protect the band degeneracies in Fe-based superconductors is one of the main results of this work. The finding allows us to characterize the form of electronic order induced by the possible effective interactions with respect to their ability to lift the band degeneracy at Γ and M points. The experimental observation of the momentum space anisotropy, temperature dependence, and domain features associated with the degeneracy lifting can then be used to determine the important microscopic electronic interactions responsible for nematicity in FeSe.

Interactions at Γ/M	Real Space	Order	Δ_Γ	Δ_M
$g_1\{(d^\dagger_{xz,e}d_{xz,e} + d^\dagger_{xz,o}d_{xz,o}) - (yz)\}$	$g_1(d^\dagger_{xz,i}d_{xz,i} - d^\dagger_{yz,i}d_{yz,i})$	Ferro-orbital	$\emptyset$	$\emptyset$
$g_2\{(d^\dagger_{xz,e}d_{xz,e} - d^\dagger_{xz,o}d_{xz,o}) - (yz)\}$	$g_2(d^\dagger_{xz,i}d_{xz,i+\delta} - d^\dagger_{yz,i}d_{yz,i+\delta})$	s-wave bond nematic	$\emptyset$	0
$g_3\{(d^\dagger_{xz,e}d_{xz,e} - d^\dagger_{xz,o}d_{xz,o}) + (yz)\}$	$g_3(-1)^{\delta_y}(d^\dagger_{xz,i}d_{xz,i+\delta} + d^\dagger_{yz,i}d_{yz,i+\delta})$	d-wave bond nematic	0	$\emptyset$
$g'_{4+}(d^\dagger_{xz,e}d_{yz,e} + d^\dagger_{xz,o}d_{yz,o}) + h.c.$	$g'_{4+}d^\dagger_{xz,i}d_{yz,i} + h.c.$	Orbital polarization	$\emptyset$	0
$ig''_{4+}(d^\dagger_{xz,e}d_{yz,e} + d^\dagger_{xz,o}d_{yz,o}) + h.c.$	$ig''_{4+}d^\dagger_{xz,i}d_{yz,i} + h.c.$	Ferro L_z/Spin orbit coupling	$\emptyset$	0
$g'_{4-}(d^\dagger_{xz,e}d_{yz,e} - d^\dagger_{xz,o}d_{yz,o}) + h.c.$	$g'_{4-}(d^\dagger_{xz,i}d_{yz,i+\delta} + d^\dagger_{yz,i}d_{xz,i+\delta}) + h.c.$	inter-orbital hopping	$\emptyset$	0
$ig''_{4-}(d^\dagger_{xz,e}d_{yz,e} - d^\dagger_{xz,o}d_{yz,o}) + h.c.$	$ig''_{4-}(d^\dagger_{xz,i}d_{yz,i+\delta} - d^\dagger_{yz,i}d_{xz,i+\delta}) + h.c.$	Orbital current/Spin orbital flux	$\emptyset$	0
$g'_{5+}(d^\dagger_{xz,e}d_{xz,o} + d^\dagger_{yz,e}d_{yz,o}) + h.c.$	$g'_{5+}e^{iQr_i}(d^\dagger_{xz,i}d_{xz,i} + d^\dagger_{yz,i}d_{yz,i})$	Charge/spin density wave	0	0
$ig''_{5+}(d^\dagger_{xz,e}d_{xz,o} + d^\dagger_{yz,e}d_{yz,o}) + h.c.$	$ig''_{5+}(d^\dagger_{xz,i}d_{xz,i+\delta} + d^\dagger_{yz,i}d_{yz,i+\delta}) + h.c.$	circulating current (flux)	0	0
$g'_{5-}(d^\dagger_{xz,e}d_{xz,o} - d^\dagger_{yz,e}d_{yz,o}) + h.c.$	$g'_{5-}e^{iQr_i}(d^\dagger_{xz,i}d_{xz,i} - d^\dagger_{yz,i}d_{yz,i})$	AF orbital	0	0
$ig''_{5-}(d^\dagger_{xz,e}d_{xz,o} - d^\dagger_{yz,e}d_{yz,o}) + h.c.$	$ig''_{5-}(d^\dagger_{xz,i}d_{xz,i+\delta} - d^\dagger_{yz,i}d_{yz,i+\delta}) + h.c.$	Ferro orbital current	0	0
$g'_{6+}(d^\dagger_{xz,e}d_{yz,o} + d^\dagger_{xz,o}d_{yz,e}) + h.c.$	$g'_{6+}e^{iQr_i}d^\dagger_{xz,i}d_{yz,i} + h.c.$	AF orbital polarization	0	$\emptyset$
$ig''_{6+}(d^\dagger_{xz,e}d_{yz,o} + d^\dagger_{xz,o}d_{yz,e}) + h.c.$	$ig''_{6+}e^{iQr_i}d^\dagger_{xz,i}d_{yz,i} + h.c.$	AF L_z/ AF spin orbit coupling	0	$\emptyset$
$g'_{6-}(d^\dagger_{xz,e}d_{yz,o} - d^\dagger_{xz,o}d_{yz,e}) + h.c.$	$g'_{6-}(-1)^{\delta_y}(d^\dagger_{xz,i}d_{yz,i+\delta} - d^\dagger_{yz,i}d_{xz,i+\delta}) + h.c.$	d-wave interorbital hopping	0	$\emptyset$
$ig''_{6-}(d^\dagger_{xz,e}d_{yz,o} - d^\dagger_{xz,o}d_{yz,e}) + h.c.$	$ig''_{6-}(-1)^{\delta_y}(d^\dagger_{xz,i}d_{yz,i+\delta} + d^\dagger_{yz,i}d_{xz,i+\delta}) + h.c.$	d-wave orbital current	0	$\emptyset$

TABLE I: The six types of effective interactions in the eigenbasis of glide symmetry (1st column), their real space representations (2nd column), physical meanings (3rd column), and whether they generate degeneracy splitting at Γ and M (4th and 5th column).

B. Degeneracy lifting interactions

On physical grounds, two degenerate states ψ_1 and ψ_2 can be split by either level shift or quantum mixing (hybridization). Using the spinor notation, $\psi = (\psi_1, \psi_2)^T$, we can express the two types of interactions as $g_z\psi^\dagger\sigma_z\psi$ and $g_x\psi^\dagger\sigma_x\psi$, respectively. The outcome of the σ_z interaction dependents on the sign of g_z, which determines

the relative position of ψ_1 and ψ_2 upon splitting and hence corresponds to two possible domains. On the other hand, the σ_x interaction, being off diagonal, leads to a hybridized spectrum symmetric in ψ_1 and ψ_2 independent of the sign of g_x, and hence produces no domain effect. Since ARPES experiments observed two-domain contributions for the splitting at M below T_s and a splitting with a single domain at Γ/Z above T_s, they must originate from two distinct type of interactions, i.e. Δ_M due to orbital shifting and $\Delta_{\Gamma/Z}$ due to quantum mixing of the orbitals.

It is therefore possible to write down all the possible forms of the electronic order or effective interactions between the degenerate orbital states at Γ and M. Since the experimental observations are generally consistent with a unit cell containing two-Fe atoms, we will focus on the interactions that do not break the lattice translation symmetry. We find six types of relevant interactions or electronic orders among the d_{xz} and d_{yz} orbitals in the eigenbasis of the glide symmetry in Eq. (8). They are listed in the first column of Table I with the corresponding coupling constants $g_1, \ldots, g_6$. The coupling constants $g_{4,5,6}$ are in general complex and are thus decomposed into real and imaginary parts by writing $g_{m\pm} = g'_{m\pm} + ig''_{m\pm}$, $m = 4, 5, 6$. In the second column of Table I, the spatial representations that produce the corresponding interactions at the Γ and M points are given. In cases where the interaction is nonlocal, we consider the nearest neighbors of site i indicated by $i + \delta_{x,y}$ along the x and y directions and the lowest angular momentum representations. The physical meaning of the electronic interaction/order is given in the third column and whether it can lift the band degeneracy at Γ and M points is noted in the last two columns of Table I.

In Table II, the matrix structures of the interactions are given explicitly in terms of the product of Pauli matrices in the orbital and sublattice subspaces. They span the complete set of the 15 generators. The columns in Table II show the properties of the corresponding interaction under the point group and glide symmetry operations given in Eqs (11) and (12). Note that although these symmetry operators can have different forms at Γ and M in the latter equations due to the presence of the reciprocal lattice vector, the symmetry and symmetry-breaking patterns of the interactions g_i are the same at Γ and M, which is consistent with the fact that the space group operations are global. However, it is important to realize that these symmetry operations can have different commutation relations at Γ and M, thus resulting in different group properties such as whether there exists a two-dimensional irreducible representation. Since the band degeneracy is protected by the newly identified antiunitary T-symmetry, it is straightforward to determine if the interaction can lift the degeneracy by breaking the $T^{\Gamma}_{1,2}$ and $T^{M}_{1,2}$ at Γ and M points separately. In the case where the degeneracy remains, the protecting T-symmetry is displayed in the parenthesis.

	g_1 $\sigma_z\tau_0$	g_2 $\sigma_z\tau_z$	g_3 $\sigma_0\tau_z$	g'_{4+} $\sigma_x\tau_0$	g''_{4+} $\sigma_y\tau_0$	g'_{4-} $\sigma_x\tau_z$	g''_{4-} $\sigma_y\tau_z$	g'_{5+} $\sigma_0\tau_x$	g''_{5+} $\sigma_0\tau_y$	g'_{5-} $\sigma_z\tau_x$	g''_{5-} $\sigma_z\tau_y$	g'_{6+} $\sigma_x\tau_x$	g''_{6+} $\sigma_y\tau_x$	g'_{6-} $\sigma_y\tau_y$	g''_{6-} $\sigma_x\tau_y$
S_4	×	×	×	×	√	×	√	√	√	×	×	×	√	√	×
Σ_d	×	×	×	√	×	√	×	√	√	×	×	√	×	×	√
G_s	√	√	√	√	√	√	√	×	×	×	×	×	×	×	×
$G_s \cdot S_4$	×	×	×	×	√	×	√	×	×	√	√	√	×	×	√
$G_s \cdot \Sigma_d$	×	×	×	√	×	√	×	×	×	√	√	×	√	√	×
Δ_Γ	∅	∅	0(∗)	∅	∅	∅	∅	$0(T_1^\Gamma)$	$0(T_2^\Gamma)$	$0(T_2^\Gamma)$	$0(T_1^\Gamma)$	$0(T_2^\Gamma)$	$0(T_2^\Gamma)$	$0(T_1^\Gamma)$	$0(T_1^\Gamma)$
Δ_M	∅	0(∗)	∅	$0(T_1^M)$	$0(T_1^M)$	$0(T_2^M)$	$0(T_2^M)$	$0(T_2^M)$	$0(T_2^M)$	$0(T_1^M)$	$0(T_1^M)$	∅	∅	∅	∅

TABLE II: Symmetry properties of the effective interactions in the direct product space of orbital and sublattice. The laster two rows indicate whether the band degeneracy at Γ and M is lifted (∅) or not (0). In the latter case, the corresponding protecting antiunitary T-symmetry is given in the parenthesis, or a $*$ is given to indicate that the interaction is identically zero at the corresponding high symmetry point.

1. $g_{1,2,3}$ interactions

Interactions $g_{1,2,3}$ produce orbital shifts as can be seen from Table I and break *both* S_4 and Σ_d symmetries while preserving G_s as shown in Table II. They are thus nematic interactions. Furthermore, since they break all the T-symmetries, the degeneracies at Γ and M are not protected and the lifting of the degeneracy must come with domain effects. Thus, $g_{1,2,3}$ are only suitable candidates for describing the observations at M points where two domains are observed by ARPES at low temperatures.

(i) The real space expression of g_1 is given in Table I,

$$O_{\rm FO} = g_1 \sum_{i\sigma} (d^\dagger_{xz,i\sigma} d_{xz,i\sigma} - d^\dagger_{yz,i\sigma} d_{yz,i\sigma}), \qquad (17)$$

which coincides with the commonly discussed ferro-

orbital order (FO) parameter. It is isotropic in momentum space and leads to $\Delta_\Gamma = \Delta_M \neq 0$ *simultaneously* by breaking all the T-symmetry, and is thus incompatible with the the experimental findings in FeSe.

(ii) As shown in Table I, g_2 is a bond operator between the nearest neighbors. In momentum space,

$$O_{\rm sNB} = g_2 \sum_{k\sigma} \gamma_k (d^\dagger_{xz,k\sigma} d_{xz,k\sigma} - d^\dagger_{yz,k\sigma} d_{yz,k\sigma}), \quad (18)$$

where $\gamma_k = \cos k_x + \cos k_y$. This is clearly an extended s-wave nematic bond order parameter that breaks both S_4 and Σ_d symmetry. The s-wave form factor (γ_k) vanishes at M point, which makes it possible for a nonzero expectation of $O_{\rm sNB}$ to generate a $\Delta_\Gamma \neq 0$ but $\Delta_M = 0$. Although this splitting patten is consistent with ARPES at $T > T_s$, $O_{\rm sNB}$ cannot describe the high temperature isotropic phase since it would break the four-fold rotation symmetry of the Fermi surface at Γ with accompanying domain effects; both were not observed experimentally.

(iii) In momentum space, the bond interaction g_3 in Table I reads

$$O_{\rm dNB} = g_3 \sum_{k\sigma} \beta_k (d^\dagger_{xz,k,\sigma} d_{xz,k\sigma} + d^\dagger_{yz,k\sigma} d_{yz,k\sigma}), \quad (19)$$

where $\beta_k = \cos k_x - \cos k_y$. This corresponds precisely to the d-wave nematic bond interaction that describes the low-temperature nematic state. $\langle O_{\rm dNB}\rangle \neq 0$ leads to $\Delta_M \neq 0$, but $\Delta_\Gamma = 0$ since its form factor β_k vanishes at the zone center. Note that $O_{\rm dNB}$ drives an *in-phase* d-wave bond order between the d_{xz} and d_{yz} orbital, which should be contrasted to the *out-of-phase* symmetry-preserving d-wave bond between these orbitals already present in the hopping terms of the TB model [35]. In the next section, we will show how $O_{\rm dNB}$ can generated by the intersite Coulomb interaction, resulting in a d-wave nematic state consistent with experimental observations at low temperatures.

2. $g_{4,5,6}$ *interactions*

The remaining 3 types of interactions, $g_{4,5,6}$ in Table I, generate quantum mixing/hybrdization among the degenerate orbitals. Thus any resulting degeneracy splitting would have only a single domain. Table II shows that although there are 4 interactions in each type with different space group symmetry properties, the degeneracy lifting pattern is the same within each type.

(i) Interactions of the g_4 type break either S_4 or Σ_d symmetry while keeping the glide symmetry G_s as seen in Table II. Thus, it is still possible for the remaining group to contain at least one two-dimensional irreducible representation. Indeed, one of the antiunitary symmetry in $T^M_{1,2}$ remains and protects the band degeneracy at M, whereas all T-symmetry is broken at Γ where the band degeneracy will be lifted as indicated in Table II. From Table I, the spin SU(2) invariant representation of g'_{4+} describes the orbital polarization due to an effective on-site crystal field correction,

$$O_{\rm OP} = g'_{4+} \sum_{i\sigma} (d^\dagger_{xz,i\sigma} d_{yz,i\sigma} + \text{h.c.}). \quad (20)$$

Similarly, that of g'_{4-} generates an inter-orbital hopping or an extended s-wave orbital polarization,

$$O_{\rm sOP} = g'_{4-} \sum_{k\sigma} \gamma_k (d^\dagger_{xz,k\sigma} d_{yz,k\sigma} + \text{h.c.}). \quad (21)$$

Although both $O_{\rm OP}$ and $O_{\rm sOP}$ split the degeneracy at Γ, the fact that they both break S_4 and $G_s \cdot S_4$ symmetries makes them incompatible with the experimental observation where the splitting at Γ in the high temperature phase maintains the four-fold rotation symmetry.

Surprisingly, the imaginary components $g''_{4\pm}$ preserves S_4 symmetry despite of $\Delta_\Gamma \neq 0$, which offers an intriguing, and the only possible account of the observed properties in the high temperature isotropic phase: degeneracy splitting only at Γ point, coexisting four-fold symmetric Fermi surfaces, and the absence of domain effects. The spin SU(2) invariant representation of g''_{4+} is

$$O_{L_z} = i g''_{4+} \sum_{i\sigma} (d^\dagger_{xz,i\sigma} d_{yz,i\sigma} - d^\dagger_{yz,i\sigma} d_{xz,i\sigma}), \quad (22)$$

which corresponds to an orbital angular momentum L_z order that breaks the time-reversal symmetry. Remarkably, there exists a time-reversal invariant but spin-SU(2) breaking representation

$$O_{\rm soc} = i g''_{4+} \sum_{i\sigma} \sigma (d^\dagger_{xz,i\sigma} d_{yz,i\sigma} - d^\dagger_{yz,i\sigma} d_{xz,i\sigma}), \quad (23)$$

which has an identical form as the spin-orbit interaction in the $d_{xz/yz}$ sector. Such an interaction can come from either the intrinsic SOC or be generated effectively [20]. Since the experimentally observed $\Delta_{\Gamma/Z}$ degeneracy splitting is nearly T-independent up to the highest measured temperature of 150K [14, 15], we conclude that the latter originates from the intrinsic atomic SOC and estimate the strength of the SOC to be on the order of 30meV. Noted that since the SOC involving all d-orbitals breaks the glide symmetry, the corresponding band crossings should be lifted except at M and A point in the BZ [29, 36]. We note that although not all such splittings have been detected at the present time, the hybridization between the d_{xy} and $d_{xz/yz}$ orbitals near Γ/Z has indeed been observed by ARPES experiments [14, 15].

The analysis of the interaction g''_{4-} in Table I can be made in the same spirit. The spin SU(2) invariant realization of this bond operator corresponds to interorbital circulating current order (or the orbital flux phase) that breaks time-reversal symmetry. Similar to $O_{\rm soc}$ in Eq. (23), there is a time reversal invariant realization that corresponds to spin-dependent orbital current order, where electrons with opposite spin-component traverse the lattice and accumulate opposite signs of the flux.

(iii) Interactions of the type g_5 and g_6 are hybridizations between the even and odd orbitals and thus break the glide symmetry G_s. The g_5 interactions are diagonal in the orbitals. The real parts represent charge density wave or spin density wave order (g'_{5+}) at wave-vector Q and antiferro (AF) orbital density wave order (g'_{5-}), while the imaginary parts are realizations of the orbital current (or flux) order (g''_{5+}) and a hybrid of ferro-orbital and orbital current order (g''_{5-}), as shown in Table I. Note that all individual interaction of the g_5 type leaves one of the T-symmetry intact at Γ and M points as seen in Table II, and thus do not lift the degeneracy at Γ and M. However, it is interesting to note that the coexistence of pairs of interactions, e.g. $g'_{5\pm}$ or $g''_{5\pm}$, would remove all the T-symmetry protections and lead to simultaneous nonzero degeneracy splitting energies at Γ and M.

(iv) The interactions of the g_6 type have the same orbital content as those of the g_4, but scatter between the even and odd components in the sublattice space. As shown in Table I, they generate AF orbital polarization (g'_{6+}), AF spin orbital coupling or AF orbital angular momentum L_z (g''_{6+}), interorbital hopping in the d-wave channel (g'_{6-}), and d-wave orbital current or flux (g''_{6-}). The degeneracy at Γ is protected by one of the remaining T-symmetry $T^{\Gamma}_{1,2}$, while it is lifted at M since all g_6 interactions are odd under $T^{M}_{1,2}$. It is important to note that although $\Delta_\Gamma = 0$ and $\Delta_M \neq 0$, g_6 cannot account for the experimental observations at low temperatures since S_4 or $G_s \cdot S_4$ remains a symmetry which implies that the Fermi surfaces maintain four-fold symmetry without nematic distortions.

Based on the systematic symmetry analysis in this section, we conclude that the distinct degeneracy lifting observed by ARPES experiments at Γ and M originate from two independent interactions: the spin-orbit interaction in Eq. (23) responsible for $\Delta_\Gamma \neq 0$ already at high temperatures above T_s and the d-wave bond nematic interaction in Eq. (19) that produces the low-temperature nematic phase with $\Delta_M \neq 0$.

III. INTERSITE INTERACTION AND d-WAVE NEMATIC BOND ORDER

In the rest of the paper, we focus on how interatomic V leads to strong band renormalization in FeSe and induces an emergent nematic order $\langle O_{\rm dNB}\rangle \neq 0$ in the ground state. To this end, we study the extended Hubbard model

$$H = H_t + H_U + H_V, \tag{24}$$

where H_t is the tight-binding (TB) model given in Eq. (1) and studied in the previous section. The intra-atomic interactions H_U are given by the standard multi-orbital Hubbard model

$$\begin{aligned} H_U &= U\sum_{i,\alpha} n_{i\alpha\uparrow}n_{i\alpha\downarrow} + (U' - \frac{1}{2}J)\sum_{i,\alpha<\beta} n_{i\alpha}n_{i\beta} \\ &- J\sum_{i,\alpha\neq\beta} \mathbf{S}_{i\alpha}\cdot\mathbf{S}_{i\beta} + J\sum_{i,\alpha\neq\beta} d^\dagger_{i\alpha\uparrow}d^\dagger_{i\alpha\downarrow}d_{i\beta\downarrow}d_{i\beta\uparrow} \end{aligned} \tag{25}$$

where U and U' are the on-site, intra- and inter-orbital on-site Coulomb repulsions and J is the Hund's rule exchange coupling with $U = U' + 2J$. Note that when the Hamiltonian (25) is used to describe the complete set of d-orbitals, J should be understood as an average of the exchange interactions of the t_{2g} and the e_g orbitals since the effects caused by the difference in the latter are usually small in a cubic system [37, 38]. The extended interatomic Coulomb interaction is given by

$$H_V = V\sum_{\langle i,j\rangle} :n_i n_j: \tag{26}$$

where the "normal-order" sign indicates that the direct Hartree term depending on the total density $n_i = \sum_\alpha n_{i\alpha}$ is subtracted, since that part of the interaction has been already included in the LDA. The same is true when treating H_U in the HF theory [25, 26]. Thus, our treatment of interactions is in the same spirit as the LDA+U+V approach [39, 40]. The importance of the extended Coulomb interaction in Fe-based superconductors has been emphasized previously [30] with a focus on the properties associated with such p-d charge transfer metals. In the down-folded Fe-only model studied here, the interatomic interaction in Eq. (26) is between the nearest-neighbor Fe atoms.

A. Quantum fluctuations due to intersite V

It is well known that the Fe-pinictides band structure is prone to a collinear SDW order that is also present in the multiorbital Hubbard model [26, 41]. Writing $\langle c^\dagger_{i\alpha\sigma}c_{i\beta\sigma'}\rangle = \frac{1}{2}[n_\alpha + \sigma m_\alpha \cos(Q_{\rm AF}\cdot\mathbf{r}_i)]\delta_{\alpha\beta}\delta_{\sigma\sigma'}$, where $Q_{\rm AF} = (\pi, 0)$ and n_α and m_α are the density and spin density in orbital α, a nonzero m_α is most easily obtained in the weak-coupling Hartree-Fock theory [41] which is reliable when U is small. Since the electron correlation strength is comparable to the bandwidth of the d-electron complex, a complete description of the collinear SDW *metal* phase with realistic parameters would require a strong coupling approach that takes into account the correlation effects nonperturbatively [26]. Here, we will carry out the Hartree-Fock theory for the extended Hubbard model in Eq. (24) using as effective parameters $U = 1.4$eV and $J = 0.2$eV. We will show that the quantum fluctuations induced by the inter-site V lead to a renormalized band structure where the Fermi level sits close to the vHS, which allows a weak-coupling approach to capture the leading instability, the suppression of collinear SDW, and the emergence of the d-wave

nematic bond order. The Hubbard interaction H_U in Eq. (25) is decoupled in terms of the self-consistent internal fields in the charge and spin sectors [26]: $\Delta_\alpha = \frac{1}{2}(2U-5J)n - \frac{1}{2}(U-5J)n_\alpha$ and $h_\alpha = \frac{1}{2}Jm + \frac{1}{2}(U-J)m_\alpha$, where $(n,m) = \sum_\alpha (n_\alpha, m_\alpha)$. The self-consistently determined ground state indeed has $Q_{\rm AF}$-SDW order *in the absence* of the inter-site interaction V. To treat the quantum fluctuations beyond LDA, we decouple H_V in Eq. (26) in the hopping/bond channel,

$$H_V = -V \sum_{\langle i,j\rangle,\alpha\beta} (\chi_{ij}^{\alpha\beta} d_{i\alpha}^\dagger d_{j\beta} + h.c. - |\chi_{ij}^{\alpha\beta}|^2), \qquad (27)$$

where $\chi_{ij}^{\alpha\beta} = \langle d_{j\beta}^\dagger d_{i\alpha}\rangle$ and the spin index is suppressed for simplicity unless otherwise noted. In the presence of translation symmetry, the real nearest neighbor valence bond between any pair of orbitals (α,β) can be decomposed into the lattice harmonics of different angular momentum in k-space:

$$\chi_{ij} = \sum_k [2\chi_s\gamma_k + 2\chi_{px}\eta_k^x + 2\chi_{py}\eta_k^y + 2\chi_d\beta_k], \qquad (28)$$

where γ_k and β_k are the extended s-wave and d-wave form factors and $\eta_k^{x(y)} = i\sin k_{x(y)}$ are the p-wave form factors. Comparing Eqs (27) and (28) to the tight-binding model in Eq.(1), it is clear that such quantum fluctuations amount to renormalizing the hopping integral

$$\mathbf{t}_{ij}^{\alpha\beta} = t_{ij}^{\alpha\beta} - V\chi_{ij}^{\alpha\beta} \qquad (29)$$

between the nearest neighbors. There are in fact two classes of contributions generated by the inter-site interaction analogous to the situation in a general renormalization group analysis: (i) the corrections to the existing hopping parameters that maintain the lattice symmetry and thus lead to the renormalization of the band structure, and (ii) the spontaneous generation of new and symmetry breaking hopping channels. Correspondingly, we can write

$$H_V = H_V^{\rm b.r.} + H_V^{\rm s.b.}.$$

Since the full expressions for $H_V^{\rm b.r.}$ and $H_V^{\rm s.b.}$ are rather lengthy, we shall display explicitly the terms involving only the t_{2g} orbitals:

$$\begin{aligned} H_V^{\rm b.r.} = &- V\sum_k 2\big[\chi_s\gamma_k(d_{xz,k}^\dagger d_{xz,k} + d_{yz,k}^\dagger d_{yz,k}) + \chi_d\beta_k(d_{xz,k}^\dagger d_{xz,k} - d_{yz,k}^\dagger d_{yz,k}) + \chi_{px}^{14}\eta_k^x d_{xz,k}^\dagger d_{xy,k} \\ &+ \chi_{py}^{24}\eta_k^y d_{yz,k}^\dagger d_{xy,k} + \chi_s^{44}\gamma_k d_{xy,k}^\dagger d_{xy,k} + h.c.] + (\text{terms involving } e_g \text{ orbitals})\big], \end{aligned} \qquad (30)$$

where $\chi_s = (\chi_s^{11} + \chi_s^{22})/2$ and $\chi_d = (\chi_d^{11} - \chi_d^{22})/2$. The symmetry-breaking part is

$$\begin{aligned} H_V^{\rm s.b.} = &- V_0\sum_k 2\big[\Delta_s\gamma_k(d_{xz,k}^\dagger d_{xz,k} - d_{yz,k}^\dagger d_{yz,k}) + \Delta_d\beta_k(d_{xz,k}^\dagger d_{xz,k} + d_{yz,k}^\dagger d_{yz,k}) \\ &+ (\chi_{px}^{11/22}\eta_k^x + \chi_{py}^{11/22}\eta_k^y) d_{xz/yz,k}^\dagger d_{xz/yz,k} + (\chi_s^{12}\gamma_k + \chi_d^{12}\beta_k + \chi_{px}^{12}\eta_k^x + \chi_{py}^{12}\eta_k^y) d_{xz,k}^\dagger d_{yz,k} \\ &+ (\chi_s^{14/24}\gamma_k + \chi_d^{14/24}\beta_k) d_{xz/yz,k}^\dagger d_{xy,k} + \chi_{py}^{14}\eta_k^y d_{xz,k}^\dagger d_{xy,k} + \chi_{px}^{24}\eta_k^x d_{yz,k}^\dagger d_{xy,k} \\ &+ (\chi_{px}^{44}\eta_k^x + \chi_{py}^{44}\eta_k^y) d_{xy,k}^\dagger d_{xy,k} + \chi_d^{44}\beta_k d_{xy,k}^\dagger d_{xy,k} + h.c. + (\text{terms involving } e_g \text{ orbitals})\big], \end{aligned} \qquad (31)$$

where $\Delta_s = (\chi_s^{11} - \chi_s^{22})/2$ and $\Delta_d = (\chi_d^{11} + \chi_d^{22})/2$. The second term in Eq.(31) is precisely the d-wave nematic interaction in Eq. (19) and the last term is its counterpart in the d_{xy} channel. Note that we have denoted the interaction strength differently as V and V_0 in Eqs (30) and (31). Although the bare values stemming from the microscopic Coulomb interaction are expected to the same, the *effective* interaction strengths $V_0 \neq V$ due to the effects of orbital polarization, screening, and other orbital dependent contributions. To develop more physical insights, we will vary V and V_0 independently around $V_0/V = 1$ in the calculations.

1. *Renormalization of the band structure in bulk FeSe*

We first discuss how V renormalizes the band structure by switching off $H_V^{\rm s.b.}$ (i.e. setting $V_0 = 0$). The evolution of the self-consistently determined low-energy band dispersions are shown in Fig. 3. With increasing V, the value of $E_{\rm vH} \simeq 350$meV in the TB model at $V = 0$ shown in Fig. 3(a) is renormalized close to the experimental value of 25meV at $V = 0.73$eV in Fig. 3(b), and then to coincide with the Fermi level E_F at $V = 0.763$eV shown in Fig. 3(c). With increasing V, notice that the Dirac crossings of the d_{xy} and $d_{yz/xz}$ bands also move up toward the Fermi level. Eventually,

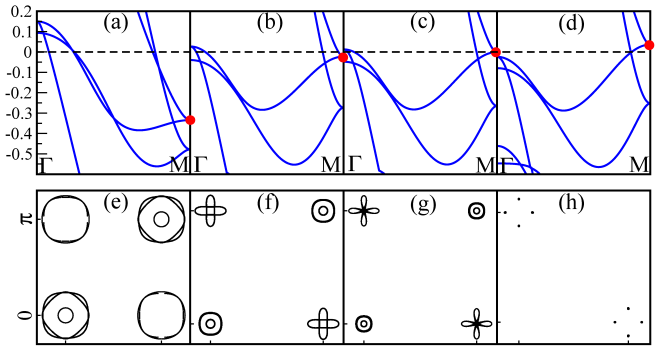

FIG. 3: Renormalized band structure (a-d) in unit of eV and corresponding FS (e-h) at $V = 0$ (a), 0.73eV (b), 0.763eV (c), and 0.85eV (d). Red dots indicate vHS at $d_{xz/yz}$ degeneracy point at M. FSs in (e) are 87.5% of their actual sizes.

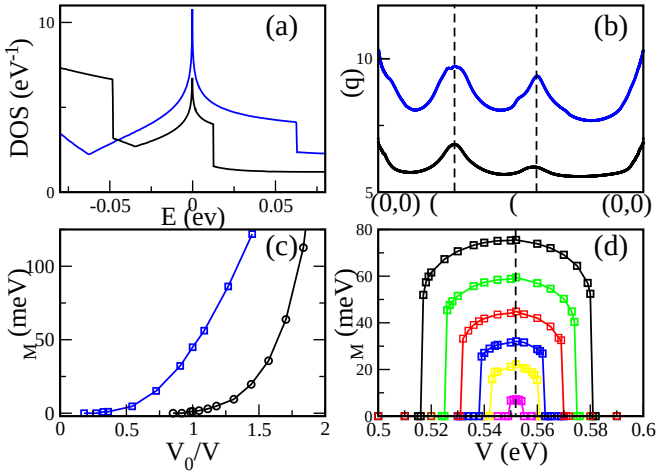

FIG. 4: DOS (a) and static susceptibility (b) of V-renormalized band structure at $E_{\rm vH} = 0$ and corresponding degeneracy-splitting energy Δ_M (c). Black lines in (a)-(c) for TB fit $t_x^{14} = 305$meV and blue line for $t_x^{14} = 100$meV. (d) Δ_M versus V around vHS for $t_x^{14} = 100$meV; curves from bottom to top are for $V_0/V = 0.6, 0.8, 0.9, 1.0, 1.1$, and 1.2. The dashed black vertical line in (d) indicates where the vHS coincides with the Fermi level.

the vHS is pushed above the Fermi level which now cuts through the Dirac nodes, while the hole bands sink below E_F at $V = 0.85$eV as shown in Fig. 3(d), realizing an interesting state of a Dirac semimetal. Correspondingly, Figs.3(e)-(h) show the remarkable evolution of the four-fold symmetric Fermi surfaces: from the very large LDA hole and electron pockets in Fig. 3(e) to the observed small elliptical electron pockets with prominent quasi-1D character in Fig. 3(f), and then to four flower pedals at $E_{\rm vH} = 0$ in Fig. 3(g), and finally to four Dirac points in Fig. 3(h).

Thus, the immediate consequence of the strong band renormalization in bulk FeSe is the dynamically generated proximity of the vHS to E_F in the electron liquid phase. It is remarkable that for the range of V values where the vHS is within 25meV of E_F in the renormalized band structure, the self-consistent solution of the ground state is always an electron liquid state that is stable against collinear SDW and charge density wave order. In Fig. 4(a), the 2D density of states (DOS) of the renormalized band at $E_{\rm vH} = 0$ is plotted, showing its logarithmic divergence at E_F. Correspondingly, the calculated two-particle static susceptibility $\chi_0(\mathbf{q})$ shown in Fig. 4(b) displays a sharp peak at $\mathbf{q} = 0$ due to the vHS, which appears even stronger than the peak at $(\pi, 0)$ which dominated the DOS in the absence of V. Thus, the electron liquid state is only unstable toward a $\mathbf{q} = 0$ nematic instability, analogous to the nematicity due to the vHS proposed for bilayer Sr-ruthenates [42]. Interestingly, we find that the vHS strengthens considerably when the hopping integral between the $d_{xz/yz}$ and d_{xy} orbitals, described by the term $-2it_x^{14}\sin(k_{x/y})d^+_{xz/yz}d_{xy}$ in the TB model, is decreased. The TB fit to LDA bands gives $t_x^{14} = 305$meV. Reducing t_x^{14} by a factor of 3 leads to a significantly flatter d_{xy} band near Γ/Z as observed in the ARPES experiments [14] and to reduced curvatures of the $d_{xz/yz}$ band at the vHS point. Figs 4(a)-(b) show that the corresponding DOS and the $\mathbf{q} = 0$ susceptibility are significantly enhanced, suggesting a much stronger nematic instability of the Pomeranchuk-type.

2. *d-wave Bond Nematic Order*

We next show that the $\mathbf{q} = 0$ instability corresponds to the d-wave nematic bond order. To this end, we first set $V = 0.763$eV where $E_{\rm vH} = 0$ (Fig.3c) and switch on V_0 in the symmetry breaking part of the Hamiltonian $H_V^{\rm s.b.}$ in Eq.(31). The self-consistent solutions show that among all the symmetry breaking terms, the leading instability occurs precisely in the d-wave nematic bond channel with nonzero Δ_d and χ_d^{44} in Eq.(31), which has the largest form factor at M-point. The degeneracy splitting energy Δ_M between the d_{xz} and d_{yz} orbitals is calculated directly from the self-consistently determined eigenstate energies at M-point and plotted in Fig. 4(c) as a function of V_0. It serves as a quantitative measure of the degree of nematicity in the ground state.

To explore the range of V over which the nematicity is controlled by the proximity of the vHS to E_F, we plot in Fig. 4(d) the Δ_M-map as a function of V for different ratios of V_0/V. The distance of the vHS to E_F, i.e. $E_{\rm vH}$, varies with V, and the dashed vertical line marks the location where the vHS sits at E_F, i.e. where $E_{\rm vH} = 0$. The most notable feature of Fig. 4(d) is the existence of plateaux nearly symmetrically distributed around $E_{\rm vH} = 0$ that grows in width and height with increasing V_0/V. For $V_0/V \sim 1$, the latter covers the experimentally observed $E_{\rm vH} \simeq 25$meV. Parallel results are obtained for $t_x^{14} = 305$meV where a similar Δ_M requires a larger V_0/V.

In Fig. 5, we plot the band dispersion and the FS calculated self-consistently in the d-wave bond nematic ground state *in a single-domain*. In Figs. 5(a)-(b), the renormalized E_F of the electron liquid is at the vHS, i.e. $E_{\rm vH} = 0$. The d-wave nematic order removes the vHS by splitting the band-degeneracy around the Fermi level and produces the 4-fold symmetry breaking FS pockets as a result of the d-wave Pomeranchuk distortion. In Figs. 5(c)-(d), $E_{\rm vH} = 25$meV in the electron liquid phase, which corresponds to the observed value for the nominally undoped FeSe. Figs. 5(e)-(f) are obtained for 1% electron doped $Fe_{1.01}Se$ which may be closer to the as-grown samples used experimentally [9, 10, 14]. In the latter two cases, we find good agreements with the measured dispersions for a single domain shown in Fig. 1(d) near the M point as well as the shape of the FS pockets [13–15].

It is important to point out that the d-wave nematic bond order and the ferro-orbital order are *not* orthogonal and mutually exclusive. They belong to the same space group as it is clear from Table II that the interactions $g_{1,2,3}$ have the same symmetry breaking pattern. As a result, both $\Delta_d = \sum_k \beta_k[n_{xz}(k) + n_{yz}(k)]$ and $\Delta_{FO} = \sum_k[n_{xz}(k) - n_{yz}(k)]$ are none-zero in the d-wave bond nematic state, deriving from a momentum distribution function $n_\alpha(k)$ that breaks the S_4 symmetry, unless additional particle-hole symmetry is present which is not the case in FeSe. The conventional Pomeranchuk FS distortion is thus generalized to the case with orbital-lattice momentum coupling. This explains why local probes such as NMR have detected FO order in the low temperature nematic phase [16, 17]. We stress that, in the present theory, the nematic transition is driven by the d-wave bond order that couples to the intersite Coulomb interaction and the FO order is induced parasitically, since the energy lowering in going from the electron liquid to the nematic state primarily comes from the d-wave nematic bond order. Indeed, since the FO order parameter $\Delta_{\rm FO}$ only couples directly to the local intra-atomic interactions but not to V, the degeneracy splitting energy $\Delta_M = 8V_0\Delta_d - \frac{1}{2}(U-5J)\Delta_{\rm FO}$ in the HF theory is dominated by the contribution from Δ_d, and even more so due to the large Hund's rule coupling J in Fe-base superconductors [26, 43] making $U - 5J$ much smaller. This explains the insensitivity of degeneracy splitting energy Δ_Γ at the zone center to the d-wave nematic bond order at low temperatures, which is estimated to have only about 5 meV variations from 120K down to 22K in the ARPES data [14], as shown in Fig. 1(d). Nevertheless, the induced $\Delta_{\rm FO}$ does lead to the distortion of the hole FS near the zone center. For the values of U and J studied here, the hole FS pockets shown in Figs 5(d), 5(f), and 5(h) near the Γ point indeed break the 4-fold rotational symmetry in a manner consistent with the experimental observations [15].

In Figs 5(g)-(h), we show the results obtained when an atomic SOC term involving the entire $3d$ complex,

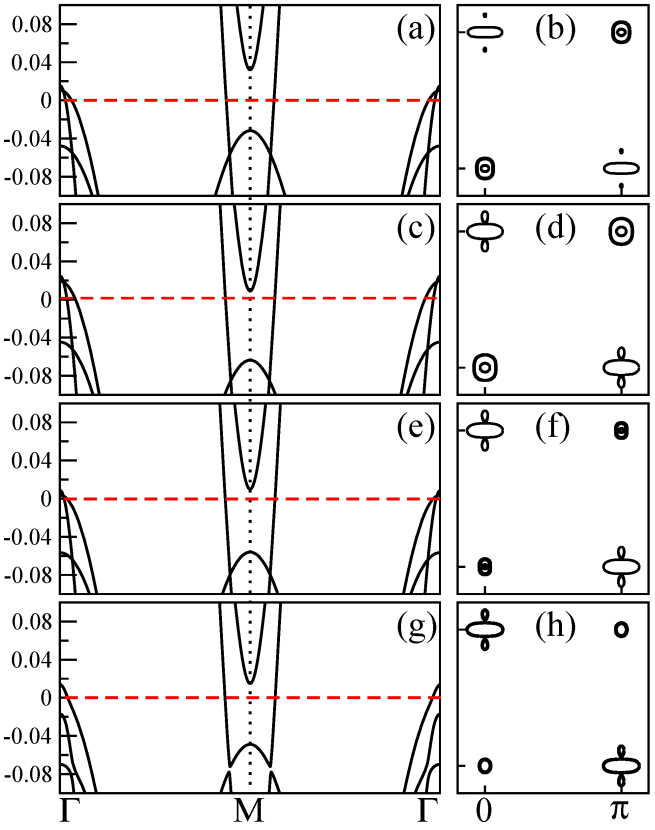

FIG. 5: Band dispersion in unit of eV (left panel) and FS (right panel) in d-wave nematic state. (a) and (b): $V = 0.763$eV, $E_{\rm vH} = 0$, and $V_0 = 1.3$eV. (c) and (d): $V = 0.73$eV, $E_{\rm vH} = 25$meV, and $V_0 = 1.34$eV. (e) and (f): $V = 0.75$ and $V_0 = 1.325$eV at 1% electron doping. (g) and (h): With SOC $\lambda_{\rm soc} = 28$meV, $V = 0.763$eV, $V_0 = 1.32$eV at 1% electron doping.

$H_{\rm soc} = \sum_{i\alpha\beta\sigma\sigma'} \lambda_{soc} \langle\alpha| L |\beta\rangle \langle\sigma| S |\sigma'\rangle d^+_{i\alpha\sigma} d_{i\beta\sigma'}$, is added to the Hamiltonian with $\lambda_{\rm soc} \simeq 28$meV. As predicted by the symmetry analysis in the last section, the SOC splits the band degeneracy at Γ without affecting the the bands at M. Moreover, it pushes one of the two hole bands at Γ below E_F, leaving a single two-fold symmetric hole pocket consistent with what was observed in ARPES and quantum oscillation experiments [13, 15]. It is important to note that since the glide symmetry is broken by the SOC, the Dirac crossings located below the Fermi level between the d_{xy} and d_{yz} orbitals in a single domain are lifted by the SOC, as shown in Fig. 5(g). This small gapping of the Dirac points can serve as a landmark for the presence of a sizable SOC in FeSe, although the detection of the d_{xy} band by ARPES below the Fermi level has been notoriously difficult in *bulk* FeSe. In contrast, we expect that Dirac like crossings formed by the d_{xy} and d_{yz} bands originating from different domains will not be gapped.

Finally, for all the cases studied with $E_{\rm vH}$ within

25meV of the Fermi level, the d-wave nematic order dominates and the collinear SDW order is absent in the self-consistent solutions of the ground state. It is thus highly conceivable that magnetism and d-wave nematicity are competing caricatures in FeSe superconductors. In the present theory, the strong band renormalization, the suppression of the collinear magnetic order, and the emergence of the electronic nematic order have the common origin which is the inter-site Coulomb interaction.

IV. SUMMARY AND DISCUSSIONS

We have shown that the rise and the demise of symmetry protected degeneracies in the electronic band structure can be used to probe the novel quantum states and the underlying interactions in correlated multiorbital electron materials. This work makes two advances in this direction with specific emphasis on Fe-based superconductors. First, a systematic symmetry analysis revealed the "hidden" antiunitary T-symmetries that protect the degeneracies at high-symmetry points in the BZ, and their connection to point-group and glide symmetry operations. This enabled the identification of the relevant electronic order/interaction that can break the T-symmetry and lift the band degeneracy. These results are applicable to all Fe-based superconductors. For bulk FeSe, the above analysis combined with recent experimental observation of the splitting of the band degeneracy, including their momentum space anisotropy, temperature dependence, and domain effects lead uniquely to the conclusion that the splitting present already in the high temperature electron liquid phase at Γ is due to the atomic SOC, while the splitting at M is due to the d-wave nematic bond order that emerges only in the low temperature nematic phase.

A microscopic theory is then developed to show that the unusually large band structure and FS renormalization, the absence of magnetism, and the emergence of the d-wave nematic order in FeSe can be explained by the important Fe-Fe interatomic Coulomb repulsion V. In addition to offering a natural description of the ARPES and quantum oscillation experiments, the theory suggests that the electronic nematicity is the driving force behind the tetragonal to orthorhombic structural transition. Interestingly, recent neutron scattering experiments in FeSe observed the spin fluctuations around $(\pi, 0)$ below the structural transition and the magnetic resonance at $(\pi, 0)$ below the superconducting transition [45, 46], which can be explained by the presence of a nematic electronic structure [47]. We also note that the same V-term has been argued recently to play an important role in stabilizing the s-wave pairing symmetry in Fe-based superconductors [44]. The overarching importance of the extended Coulomb interaction V may originate from the lack of the charge reservoir layers and the shorter Fe-Fe bond in bulk FeSe when compared to Fe-pnictides [23]. Interestingly, electronic nematicity with

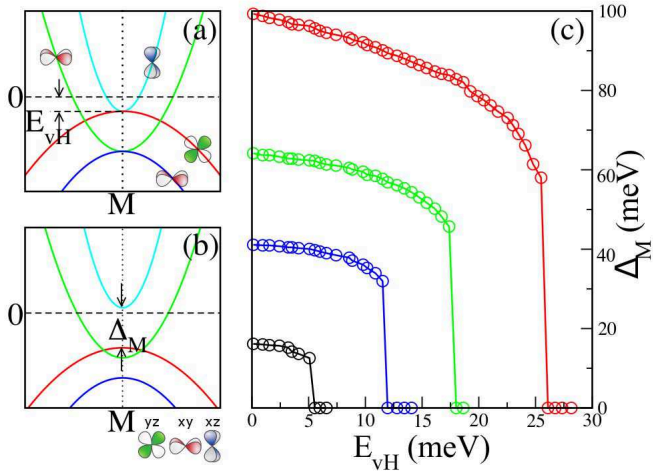

FIG. 6: (a) Schematics of the electronic structure near M showing the location of the vHS ($E_{\rm vH}$) before (a) and the degeneracy splitting energy Δ_M after (b) the nematic transition. (c) Δ_M as a function of $E_{\rm vH}$ at fixed $V_0/V = 1.8, 1.7, 1.6, 1.4$ from the top line to the bottom line.

similar phenomenology has been observed recently in 35-monolayer FeSe films with a larger $\Delta_M = 80$meV and higher $T_{\rm nem} = 125$K [48, 49], suggesting that further reduced screening of extended Coulomb interaction in films can result in a stronger V and an enhanced nematic response.

An important, falsifiable prediction of the present theory is the correlation between the emergence of the degeneracy lifting nematic state and the dynamical, inter-site Coulomb interaction V-induced proximity of the vHS to the Fermi level. It is thus desirable to seek direct experimental evidence for extended Coulomb interaction and further experimental tests by other techniques such as scanning probe and X-ray spectroscopy for the presence of the vHS near E_F above and its removal below the nematic/structural transition. This state of affairs is summarized in Fig. 6 where Δ_M is plotted versus the distance of the vHS to the Fermi level $E_{\rm vH}$ at different values of V_0. It is in principle possible to tune the vHS by doping, pressure, or chemical substitution and study the corresponding changes in the nematic response such as the transition temperature and the band degeneracy splitting energy Δ_M. While more experimental tests are clearly necessary, recent studies of chemically substituted bulk FeSe by S indeed find that Δ_M increases with decreasing $E_{\rm vH}$ [50], qualitatively consistent with the prediction shown in Fig. 6(c).

More importantly, since electron doping FeSe moves the Fermi level upward and away from the vHS at M point (see Fig. 6a), the present theory predicts that the nematic order will disappear while the vHS and band degeneracies survive at low temperatures when the material is subject to sufficient electron doping. Remarkably, this has been observed recently by ARPES on bulk

FeSe whose surface layer is heavily electron-doped with Na [51]. The measurements show that the nematic state is absent and the vHS and the band degeneracy remain intact at 65meV below the Fermi level [51]. Surprisingly, a pairing gap near E_F develops at low temperatures that is consistent with the onset of a superconducting transition at $T_c = 20$K, much higher than the 9K transition in undoped FeSe, suggesting that the nematic state in bulk FeSe is a form of competing order of the superconducting state. Furthermore, in 50-monolayer FeSe films, a continuous reduction of the nematic order induced degeneracy splitting Δ_M by surface electron doping with K has been observed, as well as an increase in the superconducting T_c when nematicity is suppressed [52].

There is indeed an empirical correlation that the higher the *electronic* nematic transition temperature, the higher the optimal superconducting T_c when electron doping removes the nematicity. Recent reports on 30-monolayer FeSe films, which are similar to the 35-monolayer films mentioned earlier with a nematic transition temperature around 125K [48, 49], shows a superconducting T_c as high as 44K [52] under K surface doping. The strongest nematic phase with $T_{\rm nem} \simeq 180$K is in fact an insulator observed in the nonsuperconducting N-phase of single and double-layer FeSe films grown on $SrTiO_3$ substrates [53, 54]. Thermal annealing introduces significant electron doping that removes the nematic insulating state in favor of the superconducting S-phase with the highest T_c as much as 65K [53–55]. Our findings on the importance of inter-site Coulomb interaction, the correlation induced proximity of the vHS near the Fermi level, and the new form of nonlocal, bond nematic orbital order with momentum space anisotropy provide considerable new microscopic insights into the intimate, competing relationship between nematicity and superconductivity, which may hold the key to understanding the pairing mechanism and to making T_c even higher in these materials.

V. ACKNOWLEDGEMENT

We thank Peng Zhang, Sen Zhou and Junfeng He for helpful discussions. This work was supported by the U.S. Department of Energy, Office of Science, Basic Energy Sciences, under Award DE-FG02-99ER45747. Z.W. thanks the Aspen Center for Physics for hospitality and the support of ACP NSF grant PHY-1066293.

[1] R. M. Fernandes, A. V. Chubukov and J. Schmalian, What drives nematic order in iron-based superconductors?, Nat. Phys. **10**, 97 (2014).

[2] C. Fang, H. Yao, W.-F. Tsai, J. Hu, and S. A. Kivelson, Theory of electron nematic order in LaFeAsO, Phys. Rev. B **77**, 224509 (2008).

[3] S. Kasahara, H. J. Shi, K. Hashimoto, S. Tonegawa, Y. Mizukami, T. Shibauchi, K. Sugimoto, T. Fukuda, T. Terashima, A. H. Nevidomskyy, and Y. Matsuda, Electronic nematicity above the structural and superconducting transition in $BaFe_2(As_{1-x}P_x)_2$, Nature **486**, 382 (2012).

[4] F. Kruger, S. Kumar, J. Zaanen, and J. Brink, Spin-orbital frustrations and anomalous metallic state in iron-pnictide superconductors, Phys. Rev. B **79**, 054504 (2009).

[5] W. Lv, J. Wu, and P. Phillips, Orbital ordering induces structural phase transition and the resistivity anomaly in iron pnictides, Phys. Rev. B **80**, 224506 (2009).

[6] C. C. Lee, W. G. Yin, and W. Ku, Ferro-Orbital Order and Strong Magnetic Anisotropy in the Parent Compounds of Iron-Pnictide Superconductors, Phys. Rev. Lett. **103**, 267001 (2009).

[7] S. Onari and H. Kontani, Self-consistent Vertex Correction Analysis for Iron-based Superconductors: Mechanism of Coulomb Interaction-Driven Orbital Fluctuations, Phys. Rev. Lett. **109**, 137001 (2012).

[8] C.-C. Chen, J. Maciejko, A. P. Sorini, B. Moritz, R. R. P. Singh, and T. P. Devereaux, Orbital order and spontaneous orthorhombicity in iron pnictides, Phys. Rev. B **82**, 100504(R) (2010).

[9] T. M. McQueen, A. J. Williams, P. W. Stephens, J. Tao, Y. Zhu, V. Ksenofontov, F. Casper, C. Felser, and R. J. Cava, Tetragonal-to-Orthorhombic Structural Phase Transition at 90 K in the Superconductor $Fe_{1.01}Se$, Phys. Rev. Lett. **103**, 057002 (2009).

[10] A. E. Bohmer, F. Hardy, F. Eilers, D. Ernst, P. Adelmann, P. Schweiss, T. Wolf, and C. Meingast, Lack of coupling between superconductivity and orthorhombic distortion in stoichiometric single-crystalline FeSe, Phys. Rev. B **87**, 180505(R) (2013).

[11] K. Nakayama, Y. Miyata, G.N. Phan, T. Sato, Y. Tanabe, T. Urata, K. Tanigaki, and T. Takahashi, Reconstruction of Band Structure Induced by Electronic Nematicity in an FeSe Superconductor, Phys. Rev. Lett. **113**, 237001 (2014).

[12] T. Shimojima, Y. Suzuki, T. Sonobe, A. Nakamura, M. Sakano, J. Omachi, K. Yoshioka, M. Kuwata-Gonokami, K. Ono, and et al., Lifting of xz/yz orbital degeneracy at the structural transition in detwinned FeSe, Phys. Rev. B **90**, 121111(R) (2014).

[13] M. D. Watson, T. K. Kim, A. A. Haghighirad, N. R. Davies, A. McCollam, A. Narayanan, S. F. Blake, Y. L. Chen, S. Ghannadzadeh, A. J. Schofield, and et al., Emergence of the nematic electronic state in FeSe, Phys. Rev. B **91**, 155106 (2015).

[14] P. Zhang, T. Qian, P. Richard, X. P. Wang, H. Miao, B. Q. Lv, B. B. Fu, T. Wolf, C. Meingast, X. X. Wu, Z. Q. Wang, J. P. Hu, and H. Ding, Observation of two distinct d_{xz}/d_{yz} band splittings in FeSe, Phys. Rev. B **91**, 214503 (2015).

[15] Y. Suzuki, T. Shimojima, T. Sonobe, A. Nakamura, M. Sakano, H. Tsuji, J. Omachi, K. Yoshioka, M. Kuwata-Gonokami, T. Watashige, and et al., Momentum-

dependent sign inversion of orbital order in superconducting FeSe, Phys. Rev. B **92**, 205117 (2015).
[16] S-H. Baek, D. V. Efremov, J. M. Ok, J. S. Kim, J. van den Brink, and B. Buchner, Orbital-driven nematicity in FeSe, Nat. Mat. **14**, 210 (2015).
[17] A.E. Bohmer, T. Arai, F. Hardy, T. Hattori, T. Iye, T. Wolf, H.v. Lohneysen, K. Ishida, and C. Meingast, Origin of the Tetragonal-to-Orthorhombic Phase Transition in FeSe: A Combined Thermodynamic and NMR Study of Nematicity, Phys. Rev. Lett. **114**, 027001 (2015).
[18] Y.-C. Wen, K.-J. Wang, H.-H. Chang, J.-Y. Luo, C.-C. Shen, H.-L. Liu, C.-K. Sun, M.-J. Wang, and M.-K. Wu, Gap Opening and Orbital Modification of Superconducting FeSe above the Structural Distortion, Phys. Rev. Lett. **108**, 267002 (2012).
[19] K. K. Huynh, Y. Tanabe, T. Urata, H. Oguro, S. Heguri, K. Watanabe, and K. Tanigaki, Electric transport of a single-crystal iron chalcogenide FeSe superconductor: Evidence of symmetry-breakdown nematicity and additional ultrafast Dirac cone-like carriers, Phys. Rev. B **90**, 144516 (2014).
[20] R. M. Fernandes and O. Vafek, Distinguishing spin-orbit coupling and nematic order in the electronic spectrum of iron-based superconductors, Phys. Rev.B, **90**, 214514 (2014).
[21] S. Mukherjee, A. Kreisel, P. J. Hirschfeld, and B. M. Andersen, Model of Electronic Structure and Superconductivity in Orbitally Ordered FeSe, Phys. Rev. Lett., **115**, 026402 (2015).
[22] Y. Su, H. Liao, and T. Li, The form and origin of orbital ordering in the electronic nematic phase of iron-based superconductors, J. Phys.: Condens. Matter **27**, 105702 (2015).
[23] H. Eschrig and K. Koepernik, Tight-binding models for the iron-based superconductors, Phys. Rev.B, **80**, 104503 (2009).
[24] A. Subedi, L. Zhang, D. J. Singh, and M. H. Du, Density functional study of FeS, FeSe, and FeTe: Electronic structure, magnetism, phonons, and superconductivity, Phys. Rev. B, **78**, 134514 (2008).
[25] S. Zhou, M. Gao, H. Ding, P. A. Lee, and Z. Wang, Electron Correlation and Fermi Surface Topology of Na_xCoO_2, Phys. Rev. Lett., **94**, 206401 (2005).
[26] S. Zhou and Z. Wang, Electron Correlation and Spin Density Wave Order in Iron Pnictides, Phys. Rev. Lett. **105**, 096401 (2010).
[27] Z. P. Yin, K. Haule, and G. Kotliar, Fractional power-law behavior and its origin in iron-chalcogenide and ruthenate superconductors: Insights from first-principles calculations, Phys. Rev. B, **86**, 195141 (2012).
[28] Z. P. Yin, K. Haule, and G. Kotliar, Kinetic frustration and the nature of the magnetic and paramagnetic states in iron pnictides and iron chalcogenides, Nat. Mat., **10**, 932 (2011).
[29] V. Cvetkovic and O. Vafek, Space group symmetry, spin-orbit coupling, and the low-energy effective Hamiltonian for iron-based superconductors, Phys. Rev. B, **88**, 134510 (2013).
[30] S. Zhou, G. Kotliar, and Z. Wang, Extended Hubbard model of superconductivity driven by charge fluctuations in iron pnictides, Phys. Rev. B, **84**, 140505(R) (2011).
[31] N. Hao and J. Hu, Topological Phases in the Single-Layer FeSe, Phys. Rev. X **4**, 031053 (2014).
[32] P. A. Lee and X. G. Wen, Spin-triplet p-wave pairing in a three-orbital model for iron pnictide superconductors, Phys. Rev.B, **78**, 144517 (2008).
[33] S. Young, and C.Kane, Dirac Semimetals in Two Dimensions, Phys. Rev. Lett. **115**, 126803 (2015).
[34] C. L. Kane and E. J. Mele, Z_2 Topological Order and the Quantum Spin Hall Effect, Phys. Rev. Lett. **95**, 146802 (2005).
[35] Breaking the glide symmetry would introduce the mixing of g_3 and g''_{5+} type of interactions that generates the dimerization between Fe_A and Fe_B as observed recently by electron diffraction [9].
[36] Symmetry analysis involving the full SOC must include the double space group. For details, see e.g. C. J. Bradley and A. P. Cracknell, *The Mathematical Theory of Symmetry in Solids* (Clarendon Press, Oxford, 1972).
[37] A. Georges, L. Medici, and J. Mravlje, Strong Correlations from Hunds Coupling, Annual Reviews of Condensed Matter Physics **4**, 137 (2013).
[38] M. E. A. Coury, S. L. Dudarev, W. M. C. Foulkes, A. P. Horsfield, P. Ma, J. S. Spencer, Hubbard-like Hamiltonians for interacting electrons in s, p and d orbitals, arXiv:1507.04613.
[39] V. L. Campo Jr and M. Cococcioni, Extended $DFT+U+V$ method with on-site and inter-site electronic interactions, J. Phys.: Condens. Matter, **22**, 055602 (2010).
[40] A. S. Belozerov, M. A. Korotin, V. I. Anisimov, and A. I. Poteryaev, Monoclinic M_1 phase of VO_2: Mott-Hubbard versus band insulator, Phys. Rev. B, **85**, 045109 (2012).
[41] R. Yu, K. T. Trinh, A. Moreo, M. Daghofer, J. A. Riera, S. Haas, and E. Dagotto,Magnetic and metallic state at intermediate Hubbard U coupling in multiorbital models for undoped iron pnictides, Phys. Rev. B **79**, 104510 (2009).
[42] S. Raghu, A. Paramekanti, E A. Kim, R. A. Borzi, S. A. Grigera, A. P. Mackenzie, and S. A. Kivelson, Microscopic theory of the nematic phase in $Sr_3Ru_2O_7$, Phys. Rev. B **79**, 214402 (2009).
[43] K. Haule and G. Kotliar, Coherence-incoherence crossover in the normal state of iron oxypnictides and importance of Hund's rule coupling, New J. Phys. **11**, 025021 (2009).
[44] J. Hu and J. Yuan, Robustness of s-wave pairing symmetry in iron-based superconductors and its implications to fundamentals on magnetically-driven high temperature superconductivity, arXiv:1506.05791.
[45] M. C. Rahn, R. A. Ewings, S. J. Sedlmaier, S. J. Clarke, and A. T. Boothroyd, Strong $(\pi,0)$ spin fluctuations in $\beta-FeSe$ observed by neutron spectroscopy, Phys. Rev. B **91**, 180501 (2015).
[46] Q. Wang, Y.Shen, B. Pan, Y. Hao, M. Ma, F. Zhou, P. Steffens, K. Schmalzl, T. R. Forrest, M. Abdel-Hafiez, X. Chen, D. A. Chareev, A. N. Vasiliev, P. Bourges, Y. Sidis, H. Cao and J. Zhao, strong interplay between stripe spin fluctuations, nematicity and superconductivity in FeSe, Nat. Mat. **15**, 159(2016).
[47] A. Kreisel, S. Mukherjee, P. J. Hirschfeld, and B. M. Andersen, Spin excitations in a model of FeSe with orbital ordering, Phys. Rev. B **92**, 224515 (2015).
[48] Y. Zhang, M. Yi, Z.-K. Liu, W. Li, J. J. Lee, R. G. Moore, M. Hashimoto, N. Masamichi, H. Eisaki, S. -K. Mo, Z. Hussain, T. P. Devereaux, Z.-X. Shen, D. H. Lu, Distinctive momentum dependence of the band reconstruction in the nematic state of FeSe thin film, arXiv:1503.01556.
[49] S. Tan, Y. Zhang, M. Xia, Z. Ye, F. Chen, X. Xie,

R. Peng, D. Xu, Q. Fan, H. Xu, and et al., Interface-induced superconductivity and strain-dependent spin density waves in $FeSe/SrTiO_3$ thin films, Nat. Mat. **12**, 634 (2013).

[50] M. D. Watson, T. K. Kim, A. A. Haghighirad, S. F. Blake, N. R. Davies, M. Hoesch, T. Wolf, and A. I. Coldea, Suppression of orbital ordering by chemical pressure in $FeSe_{1-x}S_x$, Phys. Rev. B **92**, 121108(R) (2015).

[51] J. J. Seo, B. Y. Kim, B. S. Kim, J. K. Jeong, J. M. Ok, J. S. Kim, J. D. Denlinger, C. Kim, Y. K. Kim, 20 K superconductivity in heavily electron doped surface layer of FeSe bulk crystal, arXiv:1511.07950.

[52] C. H. P. Wen, H. C. Xu, C. Chen, Z. C. Huang, Y. J. Pu, Q. Song, B. P. Xie, Mahmoud Abdel-Hafiez, D. A. Chareev, A. N. Vasiliev, R. Peng, D. L. Feng, Anomalous correlation effects and unique phase diagram of electron doped FeSe revealed by angle resolved photoemission spectroscopy, arXiv:1508.05848.

[53] S. He, J. He, W. Zhang, L. Zhao, D. Liu, X. Liu, D. Mou, Y. Ou, Q. Wang, Z. Li, and et al., Phase diagram and electronic indication of high-temperature superconductivity at 65K in single-layer FeSe films, Nat. Mat. **12**, 605 (2013).

[54] X. Liu, L. Zhao, S. He, J. He, D. Liu, D. Mou, B. Shen, Y. Hu, J. Huang, and X. J. Zhou, Electronic structure and superconductivity of FeSe-related superconductors, J. Phys.: Condens. Matter **27**, 183201 (2015).

[55] Q.Y. Wang, Z. Li, W. Zhang, Z. Zhang, J. Zhang, W. Li, H. Ding, Y. Ou, P. Deng, K. Chang, J. Wen, C. Song, K. He, J. Jia, S. Ji, Y. Wang, L. Wang, X. Chen, X. Ma and Q. Xue, Interface-Induced High-Temperature Superconductivity in Single Unit-Cell FeSe Films on $SrTiO_3$, Chin. Phys. Lett. **29**, 037402 (2012).